



저작자표시-비영리-변경금지 2.0 대한민국

이용자는 아래의 조건을 따르는 경우에 한하여 자유롭게

- 이 저작물을 복제, 배포, 전송, 전시, 공연 및 방송할 수 있습니다.

다음과 같은 조건을 따라야 합니다:



저작자표시. 귀하는 원저작자를 표시하여야 합니다.



비영리. 귀하는 이 저작물을 영리 목적으로 이용할 수 없습니다.



변경금지. 귀하는 이 저작물을 개작, 변형 또는 가공할 수 없습니다.

- 귀하는, 이 저작물의 재이용이나 배포의 경우, 이 저작물에 적용된 이용허락조건을 명확하게 나타내어야 합니다.
- 저작권자로부터 별도의 허가를 받으면 이러한 조건들은 적용되지 않습니다.

저작권법에 따른 이용자의 권리는 위의 내용에 의하여 영향을 받지 않습니다.

이것은 [이용허락규약\(Legal Code\)](#)을 이해하기 쉽게 요약한 것입니다.

[Disclaimer](#)

Master's Thesis  
석사 학위논문

Multi-axis Pressure sensor with Temperature  
Compensation based on Carbon-Composites 3D printing

Hang-Gyeom Kim(김 항 겸 金恒謙)

Department of  
Robotics Engineering

DGIST

2021

Master's Thesis  
석사 학위논문

Multi-axis Pressure sensor with Temperature  
Compensation based on Carbon-Composites 3D printing

Hang-Gyeom Kim(김 항 겸 金 恒 謙)

Department of  
Robotics Engineering

DGIST

2021

# Multi-axis Pressure sensor with Temperature Compensation based on Carbon-Composites 3D printing

Advisor: Professor Hoe Joon Kim  
Co-advisor: Professor Dongwon Yun

by

Hang-Gyeom Kim  
Department of Robotics Engineering  
DGIST

A thesis submitted to the faculty of DGIST in partial fulfillment of the requirements for the degree of Master of Science in the Department of Robotics Engineering. The study was conducted in accordance with Code of Research Ethics<sup>1</sup>

06. 28. 2021

Approved by

Professor Hoe Joon Kim  
(Advisor)

  
(signature)

Professor Dongwon Yun  
(Co-Advisor)

  
(signature)

<sup>1</sup> Declaration of Ethical Conduct in Research: I, as a graduate student of DGIST, hereby declare that I have not committed any acts that may damage the credibility of my research. These include, but are not limited to: falsification, thesis written by someone else, distortion of research findings or plagiarism. I affirm that my thesis contains honest conclusions based on my own careful research under the guidance of my thesis advisor.

Multi-axis Pressure sensor with Temperature  
Compensation based on Carbon-Composites 3D printing

Hang-Gyeom Kim

Accepted in partial fulfillment of the requirements for the degree of Master of  
Science.

05. 25. 2021

Head of Committee Prof. Hoe Joon Kim (signature)



Committee Member Prof. Dongwon Yun (signature)

A handwritten signature in black ink, likely belonging to Prof. Dongwon Yun.

Committee Member Prof. Namjung Kim (signature)

A handwritten signature in black ink, likely belonging to Prof. Namjung Kim.

## ABSTRACT

The additive manufacturing research confides in developing three-dimensional (3D) printing routes for the fabrication of devices with multifunctional materials in various interesting application areas such as self-healing, energy conversion/ storage/ harvesting, and sensing platforms. In this paper, we report the design optimization, fabrication, and characterization of a multi-axis pressure sensor with temperature compensation using fused filament fabrication (FFF) 3D printing of conductive carbon-based composites. Additive manufacturing offers a faster fabrication of complex structures with multiple properties such as electrical, mechanical, or thermal properties. The complex and costly metal printing can be neglected, as the 3D printing of a conductive polymer is a promising technology to utilize the electrical properties of the printed materials along with mechanical flexibilities. The present work focuses on the development of a multi-axis pressure sensor integrated with a temperature-sensing element. The pressure-sensing mechanism is based on piezoresistive behavior while temperature sensing relies on temperature-dependent resistance shift of the carbon composite. The pressure sensing part comprises a hollow structure to ensure mechanical deformation upon applied pressure while the temperature sensor is buried inside the housing material. Herein, the conductive three-dimensional printable polymer is synthesized by solution casting method with Polylactic acid (PLA), multi-walled carbon nanotubes (MWCNTs), and dichloromethane (DCM) solvent, which is transformed into filament for printing. The direction of pressure and magnitude of temperature can be evaluated separately by calibrating

the responses of an applied force and temperature. Moreover, an integrated temperature sensor calibrates the shift in the electrical resistance of the pressure sensor due to the alteration in environmental temperature. The additive manufactured dual pressure and temperature sensor could open up broad applications such as human motion monitoring systems and force sensing.

Keywords: 3D printing, carbon composites, pressure sensor, multi-axis sensing, temperature compensation

## List of Contents

<b>ABSTRACT .....</b>	<b>i</b>
<b>List of Contents.....</b>	<b>ii</b>
<b>List of Tables .....</b>	<b>iii</b>
<b>List of Figures .....</b>	<b>iv</b>
<b>1. Introduction.....</b>	<b>1</b>
<b>2. Overall objective .....</b>	<b>4</b>
2.1 Optimization of the 3D printable conductive polymer composite.....	4
2.2 Sensor design for multi-axis sensing and temperature compensation .....	5
<b>3. Background / Review of relevant previous work.....</b>	<b>6</b>
3.1 Piezoresistive pressure sensor .....	6
3.2 3D printing technology .....	7
<b>4. MWCNTs/PLA Fabrication &amp; Characterization .....</b>	<b>10</b>
4.1 Fabrication of MWCNTs/PLA composite filament.....	10
4.2 Characterization of MWCNTs/PLA nanocomposite .....	13
4.2.1 Sample preparation and measurement technique .....	13
4.2.2 Electrical properties of MWCNTs/PLA nanocomposite .....	15
4.2.3 Mechanical properties of MWCNTs/PLA nanocomposite .....	17
<b>5. Sensor Characterization &amp; Motion Sensing Application .....</b>	<b>21</b>
5.1 Sensor design and operation principle.....	21
5.2 Sensor characterization.....	22
5.3 3D printed multi-axis pressure sensor application .....	29
<b>6. CONCLUSION .....</b>	<b>32</b>
<b>7. REFERENCE.....</b>	<b>34</b>

## List of Tables

Table 1. 3D printing condition .....	15
--------------------------------------	----

## List of Figures

Figure 1. (a) Fabrication process of the composite filament; (b) Filament extrude process of the composite; shredded MWCNTs/PLA composite (c), and MWCNTs/PLA composite filament (d). .....	12
Figure 2. Optical images of prepared (a) filament, (b) 3D printed sample for electrical properties measurement. ....	14
Figure 3. Optical images of prepared (a) filament, (b) 3D printed sample (ASTM D638 Type V) for mechanical properties measurement. ....	14
Figure 4. (a) Electrical conductivity of the filament and 3D printed sample with MWCNTs fillers loading; (b) Relative resistance changes-temperature curve of the 3 wt% filaments and 3D printed sample. ....	17
Figure 5. Stress-strain curve of 3wt%(a) filament, (b) 3D printed specimen. (c) Young's modulus with various concentrations of MWCNTs loading. ....	19
Figure 6. Optical and SEM images of the fracture surface of (a-c) filament, (d-f) 3D printed specimen.....	20
Figure 7. 3D modeling image of (a) sensing element, (b) spacing element. (b) Optical image of an assembled multi-axis pressure sensor. (d) Operation principle of a multi-axis pressure sensor.....	22
Figure 8. (a) Bending test of the 3D printed beam structure. (b) Relative resistance change-bending strain curve of the single beam structure. (c) Loading-unloading cycle of the single beam structure. ....	23
Figure 9. (a) Relative resistance change-pressure curve for pressure sensor. (b) Base noise of the pressure sensor. (c) Relative resistance change-temperature curve for pressure sensing part(black) and temperature sensing part(red). (d) Relative resistance changes of each pressure sensing part with applied force (9.8 N) from various angle. ....	25
Figure 10. Relative resistance changes of pressure sensor, temperature sensor (a) and temperature change of the entire sensor (b) applying a force of 5 N for more the 1000 cycles. ....	27
Figure 11. Multi-axis sensing performance of pressure sensor in (a) normal force, (b) tiled force.	

.....	28
Figure 12. (a) Schematic of multi-axis pressure sensor integrated with flip-flop. (b-e) The sensing performance of the flip-flop. ....	30
Figure 13. (a) Schematic of multi-axis pressure sensor integrated with gripper. (b) The sensing performance of the gripper. ....	31

## I. Introduction

The accurate sensing of an applied force or pressure is vital for many applications including electronic skin, robotic grippers, medical tools, and clinical assessment [1, 2]. Specifically, pressure sensors are widely used to understand the gait movements of a patient, in an effort to reduce the risk of poor lifestyle or treat some medical issues associated with arthritis, hypertrophic scars, and muscular disorders [3-5]. Normal gait promotes a person to be agile for quick climbing and descending of any type of terrain. Flexible pressure sensors consist of soft body and active sensing elements have gained much attention as they offer certain benefits such as low cost, easy read-out, less complex design structure, and simple integration[6]. Such pressure sensors record the posture data of the patients and provide their motor ability, and thus enabling an correct treatment approach for each patient [7].

Three-dimensional (3D) printing technology is a simple and fast fabrication process that can produce rather complex geometries, which are hard to be produced using the conventional machining techniques. There are several methods of 3D printing such as Fused Filament Fabrication (FFF), Stereolithography (SLA), and Digital Light Processing (DLP) [8, 9]. Specifically, the FFF printing method is one of the most widely used 3D printing methods due to its cheap

equipment cost and a wide selection of materials [10]. FFF printing method can utilize both rigid and flexible polymers, such as Polylactic acid (PLA) and Thermoplastic polyurethane (TPU). Additions of novel materials can tune the properties of the 3D printed structures [11-14]. Recently, a 3D printing of conductive polymer has been used for the fabrication of electronic on various substrates [15, 16]. Also, pressure sensors by 3D printing methods using conductive polymer have been widely studied as well.

The recent development of pressure sensors has enabled many novel wearable and tactile sensing applications [17, 18]. However, many recent studies present the pressure sensors that are suited for sensing the single direction force, generally in normal direction, instead of realizing the multi-axis sensing capability [19]. In reality, to sense body motion perfectly, it is necessary to sense the normal force as well as the forces applied from various angles/ directions. Furthermore, most of the conductive polymer composites possess the property of changing their resistance according to temperature [20]. Such temperature effect can be even more troublesome for MWCNTs, which is one of the most widely used conductive fillers for 3D printing, due to their both metallic and semiconducting nature [21]. Therefore, for accurate measurement and control of the pressure sensor, one should account for such a temperature effect and

alleviate it.

In this present report, we overcome such problems by integrating a bumper structure and three pressure sensing parts for a multi-axis pressure analysis and a temperature sensing part for calibration. In addition, we show the MWCNTs/PLA composite characterization and the optimization of the material for 3D printing. Dual nozzle FFF 3D printer fabricates a multi-axis pressure sensor capable of temperature compensation. The developed multi-axis pressure sensor with an integrated temperature sensor was tested for various electrical and mechanical characterization along with a cyclic loading test to confirm its stability. The pressure sensing part results in different readings when a tilted force is applied, and the embedded temperature sensor can accurately monitor the environmental temperature. The proposed sensor mounted flip-flop can distinguish various body motions. Also, the designed sensor is integrated with the gripper for measuring the grasp force as well as the weight of the object.

## **II. Overall Objective**

This thesis includes two objectives: (1) the optimization of printing MWCNT/PLA conductive polymer using FFF method, and (2) Sensor design for multi-axis sensing and temperature compensation. Upon thorough these objectives, we will be able to make a multi-axis pressure sensor with temperature compensation based on conductive polymer 3D printing.

### **1) Optimization of the 3D printable conductive polymer composite**

The composite polymers are containing conductive fillers such as AgNW, carbon black, graphene, and carbon nanotube act as major building blocks for flexible electronics [22-26]. Especially MWCNTs possess excellent mechanical and electrical properties along with lower costs compared to other candidate materials mentioned above. In addition, MWCNTs have a high aspect ratio, which is advantageous to form conductive networks in the polymer matrix. So, they are showing a relatively low electrical percolation threshold. Furthermore, PLA offers reliable and precise printing utilizing FFF 3D printers, and it is also biodegradable. In this paper, we investigate the impacts of MWCNT concentration on the electrical, mechanical, and thermal properties of the composites. In addition, we compare the results of the mixed composite with the printed specimen and analyze the impact of printing on material properties.

## **2) Sensor design for multi-axis sensing and temperature compensation**

Accurate measurement of applied force or pressure is in much need for human and robotics motion sensing. Moreover, the recent development of flexible pressure sensors has enabled many novel wearable and tactile sensing applications. However, many recent studies present the pressure sensors that are suited for sensing the single direction force, a generally normal direction, instead of realizing the multi-axis sensing capability. In reality to sense body motion perfectly, it is necessary to sense the normal force as well as the forces applied from various angles. Furthermore, most of the conductive polymers have the property of changing their resistance according to temperature [27]. Such temperature effect can be even more troublesome for MWCNTs, due to their both metallic and semiconducting nature. Therefore, to accurately measure pressure, one should account for such temperature effect and alleviate it. In this work, we tackle this problem by integrating a MWCNTs/PLA element that does not deform upon pressure, so its resistance just varies by temperature changes. In conclusion, we propose the multi-axis pressure sensor capable of temperature compensation by combining the temperature sensing element.

### **III. Background / Review of Relevant Previous Works**

#### **1) Piezoresistive pressure sensor**

There are three main types of pressure sensing mechanisms: piezoresistive, capacitive, and piezoelectric [6, 28]. Capacitive pressure sensors measure pressure by measuring the change in capacitance between the electrodes. They show low hysteresis and good repeatability. However, it is difficult to measure the electrical signal and the noise level is very high. Piezoelectric pressure sensors measure the pressure the charge generated from certain active materials when pressure is applied. They exhibit low power consumption, but it cannot measure continuous force. The piezoresistive effect is the change in electrical resistivity due to mechanical deformation. The piezoresistive pressure sensor is the pressure sensor using the piezoresistive effect. When an external force is applied to the pressure sensor, mechanical deformation occurs, and its electrical resistivity changes. Hence one can quantify the applied stress by calibrating the recorded shift in electrical resistance. The piezoresistive pressure sensor has been widely studied due to the advantages of its simple structure, stable signal output, and vast choices of materials [17, 29]. However, the resistance of a piezoresistive pressure sensor changes according to temperature, which needs to be calibrated [27, 30, 31]. To solve this problem, we have

integrated temperature sensor which is independent of applied force for temperature compensation. The pressure range for sensing pressure at the body interface is mainly distributed in low pressure (<10 kPa) and medium pressure (10-100 kPa). The low pressure range is mainly caused by activities such as gripping and picking up objects. In addition, in the case of medium pressure, it primarily occurs at the plantar pressure of the body weight [19]. This study focuses on a sensing range of 0.1~50 kPa to sense body motion in daily activities. Here, we use 3D printing technology to make pressure sensors easier and faster. Moreover, It has the advantage of being able to flexibly control the detection range of the target pressure as the design parameters can be easily modified.

## **2) 3D printing technology**

3D printing technology, also known as additive manufacturing, is a simple and fast fabrication process by stacking layers that can produce rather complex geometries, which are hard to be produced using conventional machining techniques [32]. There are several methods of 3D printing such as Fused Filament Fabrication (FFF), Stereolithography (SLA), and Digital Light Processing (DLP) [8, 9]. In the case of FFF, the molding occurs by melting a solid polymer by

heat and extruding it under a certain pressure, In the case of SLA and DLP, it utilizes localized curing of photocurable resins by UV irradiation. Direct Ink Writing (DIW) produces a structure by extruding a droplet or paste type of ink at constant pressure through a nozzle [33]. Among the aforementioned methods, the FFF printing method is one of the most widely used 3D printing methods due to its cheap equipment cost (the equipment part is also affordable and do not have to be manufactured in a large facility) and a wide selection of materials (wide range of thermoplastics and ceramic filament) [10]. The other reasons for considering the FFF printing technology from other approaches are its speed (any CAD drawing can be transformed into finished products only in one step), accuracy (it uses a thermoplastic which is first heated up to the melting point and further extracted as layers. The accuracy is estimated to be 0.005 inches), scaling (users can scale the part down to fit the required production space without losing the accuracy) [34-37]. FFF printing method can utilize both rigid and flexible polymers, such as Polylactic acid (PLA) and Thermoplastic polyurethane (TPU). Additions of novel materials can tune the properties of the 3D printed structures [11-14, 38]. Recently, a 3D printing of polymer with electrically conductive nanowires or particles has been used for the fabrication of electronic on various substrates [15, 16]. Some of the past literature also used the 3D printing

approach to design pressure sensors [39-41]. The FFF printing method serves as an effective method to print any composite-based physical sensors due to its extensive benefits by being quite flexible and the technology allows small overhangs using the support from lower layers [42-45]. Wang et al. [46] reported 3D printed stretchable pressure sensor using TPU/CB/NaCl for sensing material and TPU/Ag for electrode material. Kim et al. [47] reported 3D printed multi-axial force sensor using CNT/TPU nanocomposite filament. Furthermore, Guo et al. [48] fabricated full 3D printed tactile sensor using Ag/silicone ink. In most previous studies, they focus on only a single direction sensing. However, to accurately sense body or robotics motion, multi-axis sensing is very necessary. To solve this problem, we have used bumper-spacing structure for multi-axis pressure sensing.

## IV. MWCNTs/PLA Fabrication & Characterization

### 1) Fabrication of MWCNTs/PLA composite filament

Figure 1 (a) shows the fabrication process of MWCNTs/PLA filament. MWCNTs can control their length and diameter in accordance with synthesis method. Their electrical, mechanical, thermal properties are different depending on length and diameter. In the case of MWCNTs composite, longer and thicker MWCNTs ensure a more effective electron conduction path. On the other hand, the mechanical properties of MWCNTs composite is dependent of aspect ratio of MWCNTs [49-52]. Figure 1(a) shows the fabrication process of the composite filament from the base materials. In this study, we have used commercial MWCNTs powder (JEIO Inc., Jentube 10A, Korea) with diameter 8~13 nm, length 100~200  $\mu\text{m}$ , and their aspect ratio is approximately  $10^5$ . MWCNTs powder is dispersed in the dichloromethane (DCM) solvent using a probe-type ultrasonicator (Bio konvision, BKUP-600K) at 24.86 kHz, 180 W for 5 min. Further, the PLA pellet is dried in a vacuum oven at 60 °C for 24 hours to restrict the presence of any moisture. 50 g of PLA pellets (Pureco Inc., P1909, Korea) are dissolved in 500 ml of the MWCNTs/DCM suspension by magnetic stirring at 600 rpm at ambient temperature for 8 hr. It was then transferred into an oven for solvent evaporation. The evaporation of DCM solvent

is performed at 100°C for 12 hr using a convection oven. Finally, the dried MWCNTs/PLA composite is ground using a mixer grinder (Figure 1(c)). The MWCNTs/PLA filament was obtained using an extruded filament with 2.8 mm comprising of a single screw extruder (Well-zoom line II, China) at 180°C. The extrusion speed was 45 cm/min. Figure 1(b) shows the extrude of the MWCNTs/PLA composite filament and Figure 1(d) shows the fabricated filament.

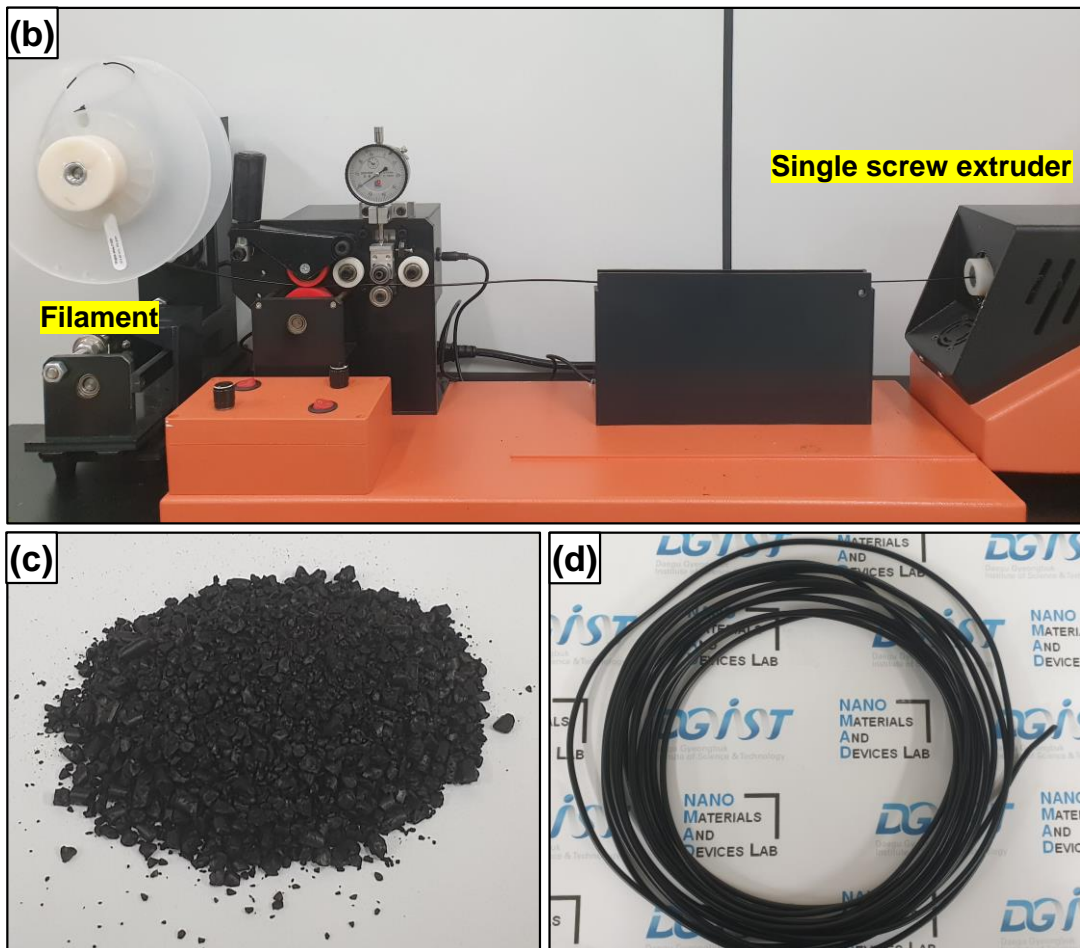
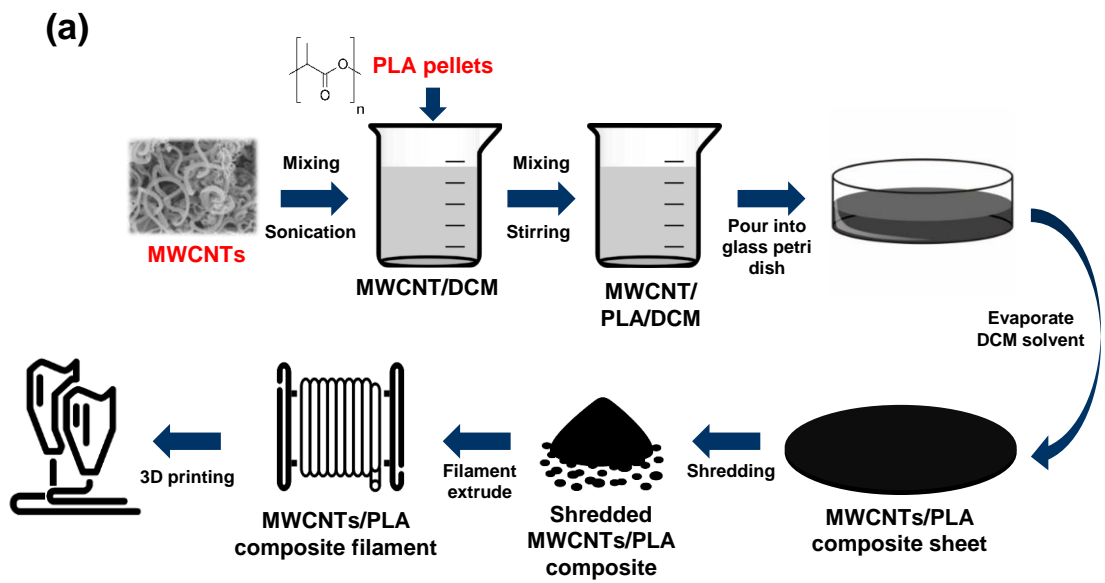
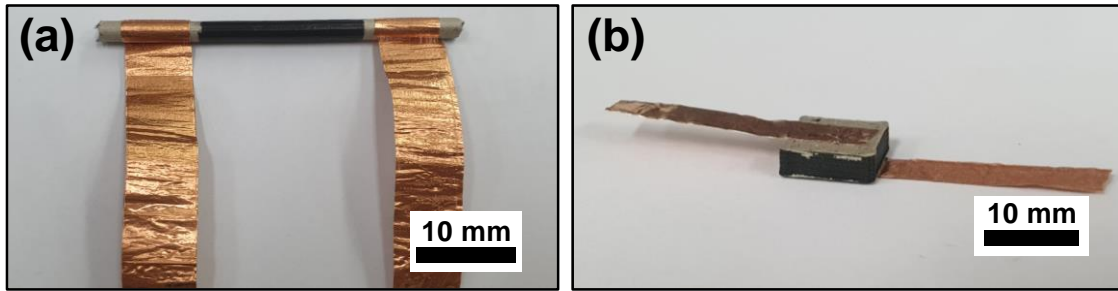


Figure 1. (a) Fabrication process of the composite filament; (b) Filament extrude process of the composite; shredded MWCNTs/PLA composite (c), and MWCNTs/PLA composite filament (d).

## **2) Characterization of MWCNTs/PLA nanocomposite**

### **Sample preparation and measurement technique**

For electrical and thermal property characterization of PLA/MWCNT composites, we have prepared the filament and 3D printed sample for MWCNT weight percentages (wt%) from 0% to 4%. In general, FFF 3D printer uses brass nozzles. However, when printing CNT composite, there is a concern that the nozzle wears due to high Young's modulus of CNT[15]. To avoid this problem, we use 0.6 mm ruby nozzle. Figure 2 shows the prepared both samples for electrical properties measurement, the filament sample (Figure 2(a)) is cut into a length of 55 mm, and then it is coated with conductive epoxy (CircuitWorks, CW-2400) at both ends and further heated in a convection oven at 60 °C for 4 hr to cure the conductive epoxy followed by attaching the copper tape. The 3D printed sample is printed in 10 x 10 x 3 mm (width x depth x height) (Figure 2(b)) structure using a FDM 3D printer (Ultimaker, Ultimaker S3, Netherland) (layer height: 0.2 mm, printing speed: 45 mm/s, line width: 0.5 mm) bearing a dual nozzle. Then, the conductive epoxy is coated on both sides of the surfaces followed by attaching the copper tape to form electrical contacts.



**Figure 2. Optical images of prepared (a) filament, (b) 3D printed sample for electrical properties measurement.**

Figure 3 shows samples for mechanical properties measurement. The filament sample (Figure 3(a)) is prepared with a length of 70 mm, and the 3D printed sample (Figure 3(b)) is printed out based on the ASTM D638 Type V specimen (Length: 9.53 mm, Width: 3.18 mm, and thickness: 3.2 mm).

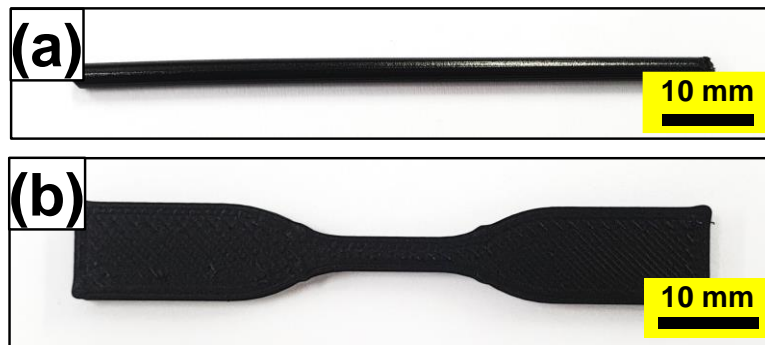


**Figure 3. Optical images of prepared (a) filament, (b) 3D printed sample (ASTM D638 Type V) for mechanical properties measurement.**

The surface morphology of the samples is taken using a scanning electron microscope (Hitachi-S-4800, Japan). The resistance is measured using the digital multimeter (Agilent, 34401A, USA). Temperature is controlled by a convection oven (JS research Inc., JSOF-150, Korea), and a thermocouple (Keysight, U1186A) is used for accurate temperature monitoring.

Electrical measuring data is acquired by NI LabVIEW 2016 program (National Instruments Corp.). Tensile testing and compression test are performed using Universal Testing Machine (KMNT Inc., KU7000M-1A, Korea). The crosshead speed for the tensile test is 0.5mm/min.

The 3D printing conditions are specified in Table 1.

<b>Material</b>	<b>Printing temperature</b>	<b>Printing speed</b>	<b>Line width</b>	<b>Nozzle Size</b>	<b>Layer height</b>
<b>Commercial TPU filament</b>	240°C	25 mm/s	0.38 mm	0.4 mm (Brass nozzle)	0.2 mm
<b>MWCNTs/PLA nanocomposite</b>	230°C	45 mm/s	0.5 mm	0.6 mm (Ruby nozzle)	

**Table 1. 3D printing condition.**

### **Electrical properties of MWCNTs/PLA nanocomposite**

As author has mentioned above, MWCNTs possess excellent mechanical and electrical properties along with lower costs. Also, MWCNTs well form percolation networks in polymer matrix due to their high aspect ratio. Figure 4(a) shows the electrical conductivity of the filament and 3D printed sample at various MWCNTs concentrations ranging from 0 to 4 wt%. The conductivity of each sample is calculated using the following equation:

$$\sigma_{Filament} = \frac{1}{R_{Filament}} \times \frac{l}{\pi \times \left(\frac{D}{2}\right)^2}$$

$$\sigma_{3D-printed} = \frac{1}{R_{3D-printed}} \times \frac{H}{A}$$

where:  $l$  is the length of the between the coated conductive epoxy and  $D$  is the diameter of filament;  $H$  is height and  $A$  is the area of coated conductive epoxy of 3D printed sample.

In the case of the composite filament, the electrical conductivity increased rapidly at 0.5 wt% of filler contents, and a fully percolated MWCNTs network is shown at over 1 wt% of filler contents. This result depicts that the MWCNTs/PLA composite is consistent with the previously reported percolation theory [53], and through this, the conductive networks are well-formed between the PLA matrixes when the MWCNTs fillers are loaded over 1 wt%. In the 3D printed sample, the electrical conductivity also increased with the amount of MWCNTs. However, their electrical conductivity value is lower than that of the filament, caused by the voids between the 3D printed layers and incomplete layer interaction. Figure 4(b) shows the change in the relative resistance for 3wt% of filament and 3D printed sample as a function of the temperature. Intrinsic MWCNTs fillers have a negative temperature coefficient of resistance (TCR), showing the semiconducting nature of MWCNTs [21, 54]. In the case of the filament, the resistance decreases with increasing temperature up to 75°C, and further the resistance increases

due to thermal expansion of the polymer matrix. However, in the case of the 3D printed sample, its resistance increases from 40°C. This may be due to the residual thermal stress, produced during the 3D printing process, in the sample and it expedites the thermal expansion at a lower temperature compared to the filament sample [55]. Therefore, there is a discrepancy in thermal behaviors between the filament and 3D printed samples. The electrical resistance of the temperature sensing part only depends on the environmental temperature and is thus suited for temperature calibration during the sensor operation.

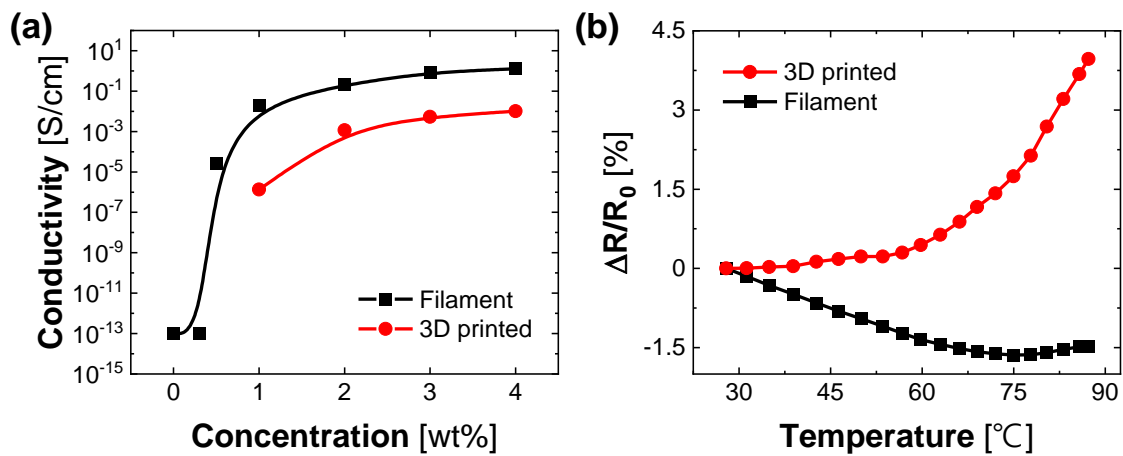


**Figure 4. (a) Electrical conductivity of the filament and 3D printed sample with MWCNTs fillers loading; (b) Relative resistance changes-temperature curve of the 3 wt% filaments and 3D printed sample.**

### **Mechanical properties of MWCNTs/PLA nanocomposite**

In terms of mechanical properties, the MWCNT fillers act as reinforcement agents in the polymer matrix. Figure 5(a) shows Young's modulus of the filament and 3D printed specimen

for each filler content. For both filament and 3D printed specimens, the addition of 4 wt% filler increased Young's modulus by 41.57% and 59.34%, respectively. This is because the external stress applied to the composite is delivered and distributed along the MWCNTs in the polymer matrix, increasing Young's modulus. In addition, Figure 5(b, c) shows the stress-strain curves of the 3wt% filament and the 3D printed sample. In the filament, necking occurred at 6% strain and fracture occurred at 15% strain. However, the 3D-printed sample fractured at 8% strain without any necking. Young's modulus of the 3D printed samples is lower than the filament.

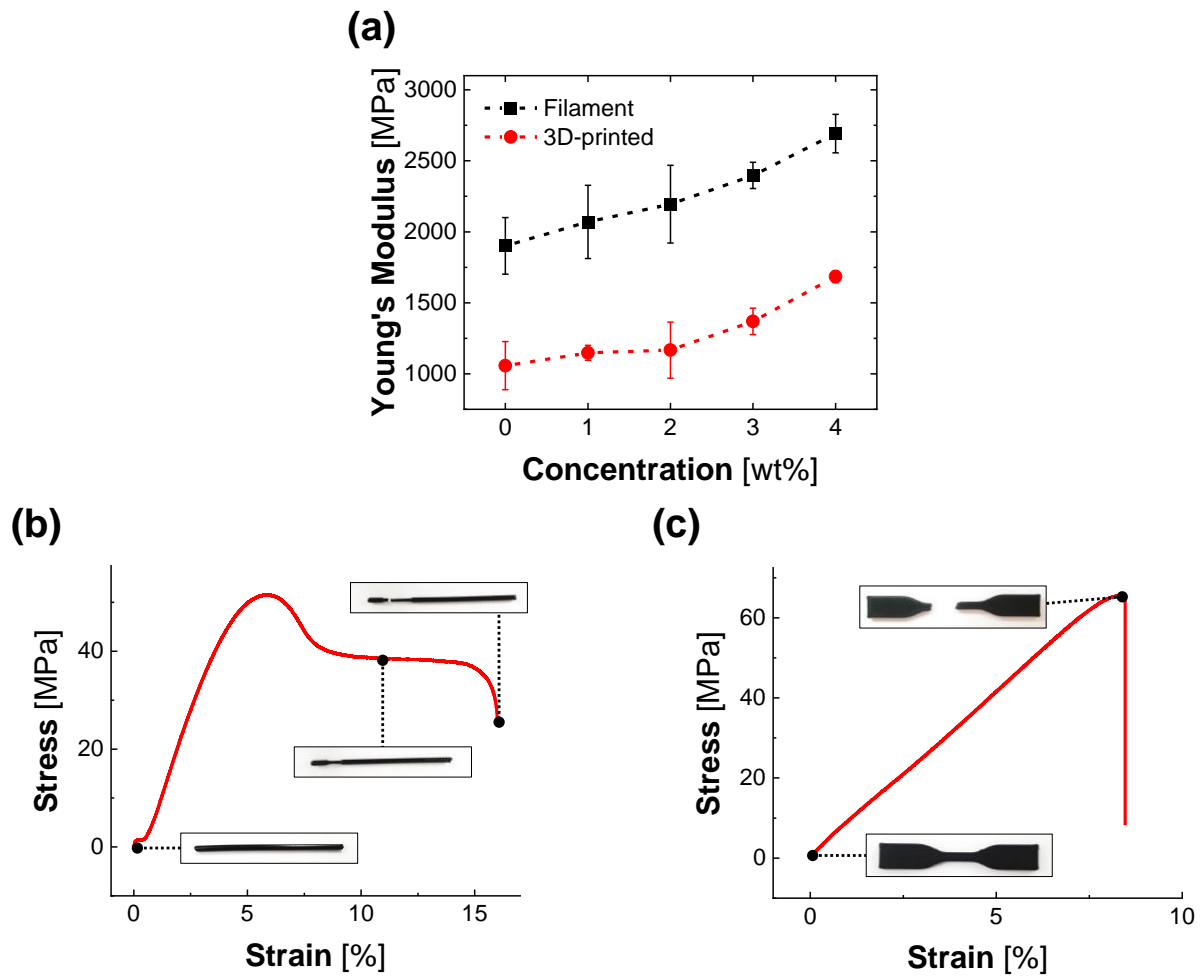


**Figure 5. Stress-strain curve of 3wt%(a) filament, (b) 3D printed specimen. (c) Young's modulus with various concentrations of MWCNTs loading.**

The digital picture of the filament and 3D printed structure is shown in Figure 6. The surface morphology of the fabricated structures is shown in Figure 6(b, c, e, and f). Unlike the filament, in the case of 3D printed samples, they bear incomplete interfacial bonding between the layer by layer and voids between layers. Such voids and interlayers in 3D printed samples could lower Young's modulus. However, it is depicted that the addition and control of MWCNT wt% can tune the mechanical properties of the 3D printed composites. The 3 wt% of MWCNTs/PLA

is chosen for 3D printing due to its high electrical conductivity and suitable mechanical properties. Figure 6(e, f) the presence of voids in the wider raster of the printed sample and the temperature difference between the previously deposited raster and later deposited raster in the process of melting and solidifying can lead to weakening the bonding between the printed layers causing the brittle fracture of the 3D printed composites [56, 57].

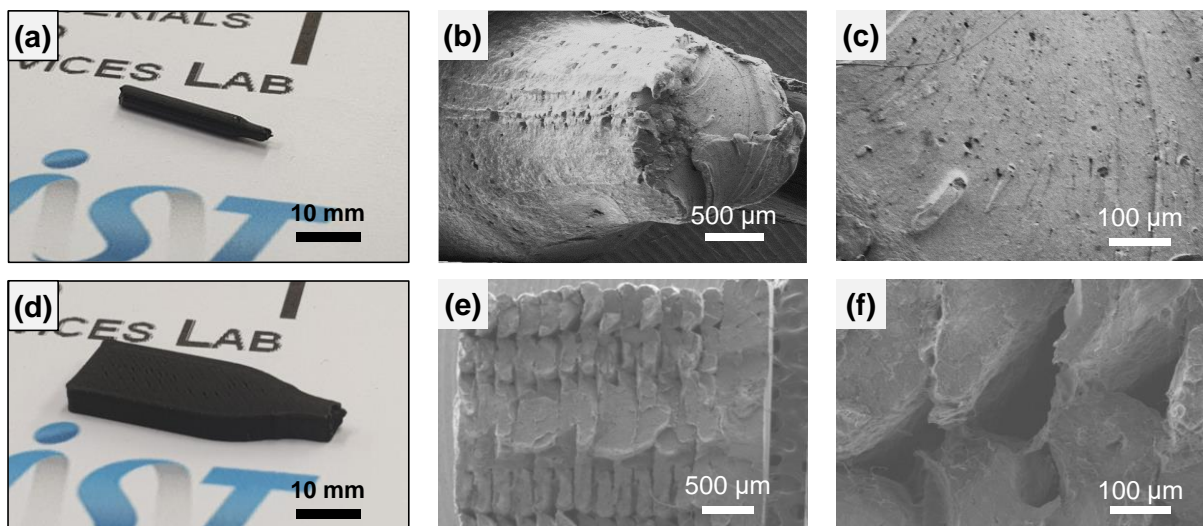


**Figure 6. Optical and SEM images of the fracture surface of (a-c) filament, (d-f) 3D printed specimen.**

## **V. Sensor Characterization & Motion Sensing Application**

### **1) Sensor design and operation principle**

We have designed the sensor with bumper-spacing structure for multi-axis force sensing. Our sensor is made by assembling the above sensing element (Figure 7(a)) and the below spacing element (Figure 7(b)), both 3D printed. A double-sided PI tape has been utilized for its assembly. TPU has Young's modulus of 26 MPa, and sufficiently deforms under an applied force so it is employed as the main body material of the sensor. The digital photograph of the fabricated sensor is shown in Figure 7(c). The sensing element uses a bumper structure with a hollow channel beneath so that the pressure sensing parts have different degrees of mechanical deformation depending on not only the magnitude, but also the direction of the applied force (Figure 7(d)). The temperature sensing part is placed independently concerning the pressure sensor. In such a way, the response of the pressure and temperature sensor is differentiated. The proposed sensor design ensures that the resistance change in the temperature sensing part is not due to mechanical deformation. Moreover, we can control pressure sensing range by changing sensor design parameters such as TPU and MWCNTs/PLA thickness of the above sensing element. In this study, we were using 1.4 mm of TPU and 0.2 mm of MWCNTs/PLA.

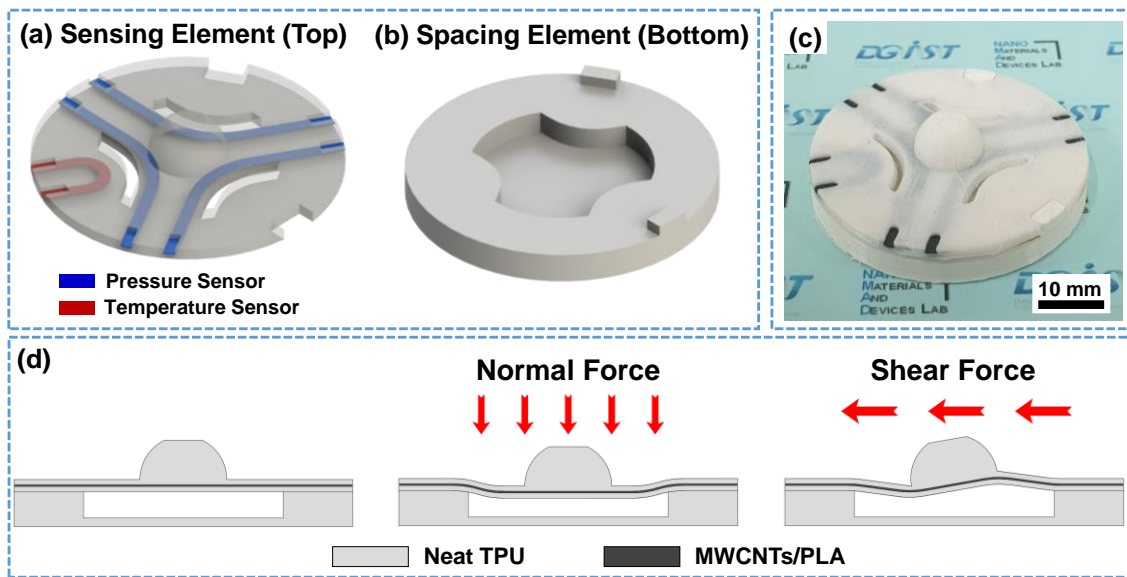


**Figure 7. 3D modeling image of (a) sensing element, (b) spacing element. (b) Optical image of an assembled multi-axis pressure sensor. (d) Operation principle of a multi-axis pressure sensor.**

## 2) Sensor characterization

We propose a beam structure to measure the resistance change as function of strain of MWCNTs/PLA composite. Figure 8(a) shows the digital image of the 3D printed beam structure model. Here the structure material is fabricated using a commercial TPU filament and sensing material is formed with 3wt% of MWCNTs/PLA composite filament. Figure 8(b) shows the relative resistance change with bending strain. The resistance linearly increases up to 0.28 % bending strain. After about 0.3% bending strain, the sensor resistance increases sharply as the MWCNT network becomes unstable at such a high strain. This can be improved by implementing a softer material to build the sensor. Figure 8(c) shows the loading-unloading

cycle for 0.53 mm displacement. The sample recovered its original electrical resistance after the loading test. Such results indicate that the resistance changes linearly as the MWCNTs/PLA composite is strained, and the recovery of the resistance is stable.

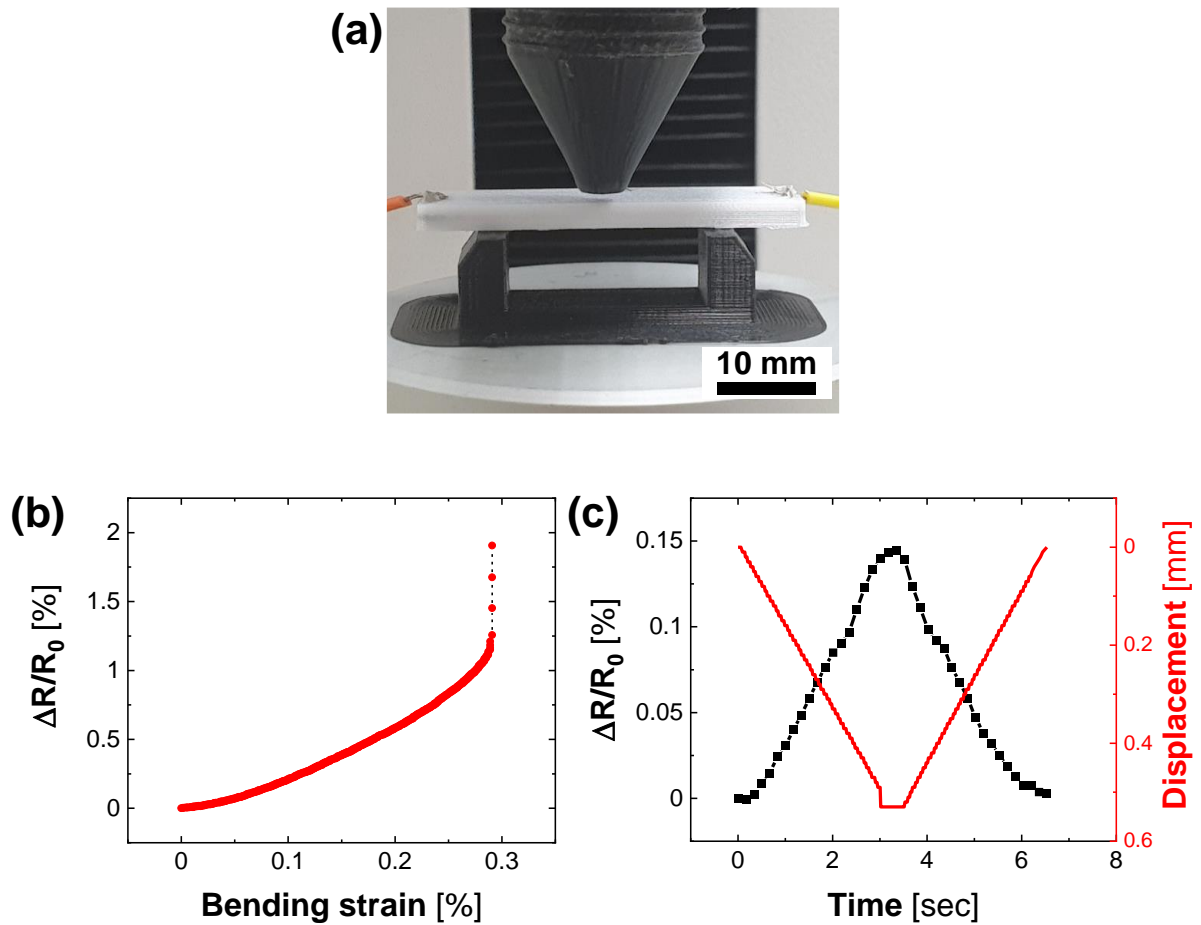


**Figure 8. (a) Bending test of the 3D printed beam structure. (b) Relative resistance change-bending strain curve of the single beam structure. (c) Loading-unloading cycle of the single beam structure.**

Figure 9(a) shows the relative resistance change of the pressure sensing part of the built sensor as a function of the applied normal pressure. The relative resistance change is divided into two linear regions. The sensor shows a sensitivity of  $2.689 \times 10^{-4}$  /kPa up to 2.2 kPa. The

junctions of the conductive networks in the polymer matrix get rapidly disconnected as excessive pressure is applied and results in a higher sensitivity of  $21.240 \times 10^{-4}$  /kPa at a higher pressure range. Figure 9(b) shows the base noise of the pressure sensing part. Limit of detection (LOD) value is one of the important factors that determine the performance of the pressure sensor. LOD value is calculated using the following equation:

$$\text{LOD} = 3.3 \times \frac{S_y}{S} = 3.3 \frac{1.308 \times 10^{-5}}{1.18 \times 10^{-3} \text{ /kPa}} = 36.58 \times 10^{-3} \text{ kPa} = 36.58 \text{ Pa}$$

where:  $S_y$  is standard deviation of the base noise (Figure 9(b)),  $S$  is slope of the Relative resistance change-pressure curve with applied tiny force to pressure sensor (Figure 9(c)).

Our sensor shows 36.58 Pa of LOD value and up to 30 kPa of sensing range. This means our sensor is susceptible to a noise level and can cover a wide sensing range. So, our sensor can use it for daily activities as well as for high-sensitivity e-skins. Moreover, 3D printing technology is relatively easy to modify the design parameters. Therefore, we can control the target pressure sensing range more easily by adjusting the sensor design parameters. Figure 9 (d) shows the relative resistance change according to the temperature change in pressure and temperature sensing parts. The resistance decreases up to 40°C following the expected negative TCR of MWCNTs. However, the resistance starts to increase around 40 °C due to the thermal

expansion of the polymer matrix. It shows that for both pressure and temperature sensing parts, the sensor resistance behaves similarly. Figure 9 (e) shows the change in resistance when a force of 9.8 N is applied to the sensor at different angles. At an angle of 50 degrees, the difference in resistance between  $R_1$  and  $R_2$  is 0.121 %. This shows that both the magnitude and direction of an applied force can be calibrated by analyzing the response of each pressure-sensing element.

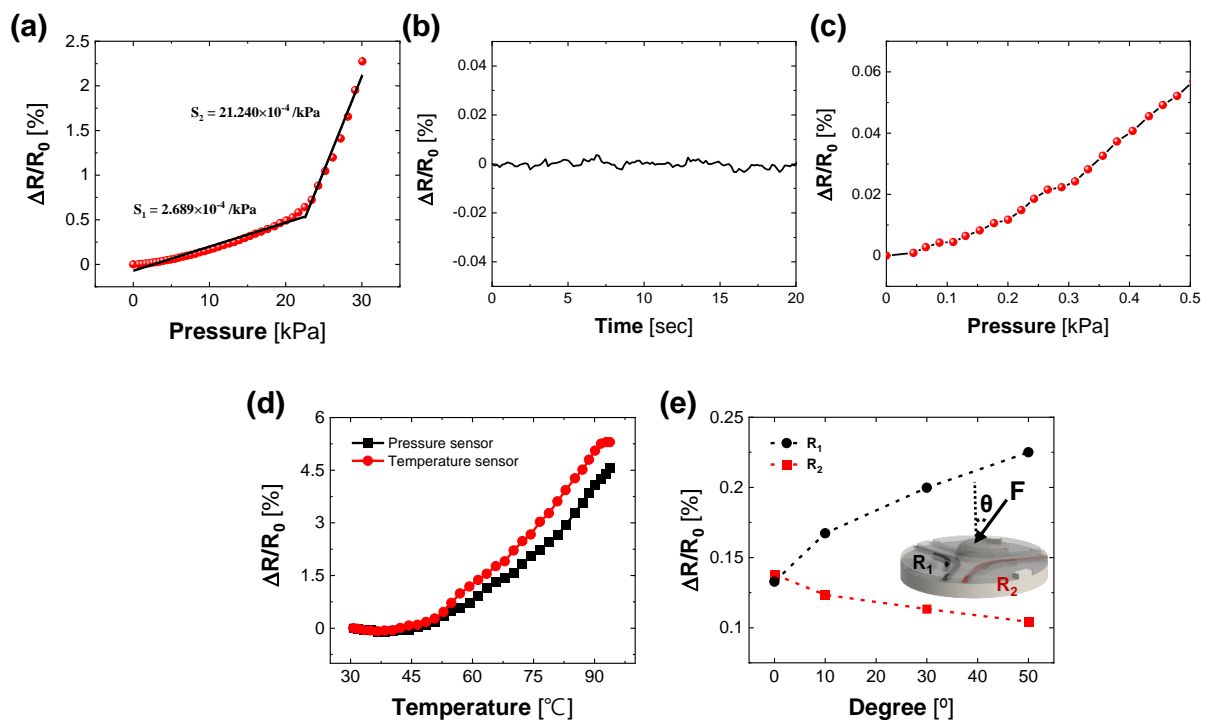


**Figure 9.** (a) Relative resistance change-pressure curve for pressure sensor. (b) Base noise of the pressure sensor. (c) Relative resistance change-pressure curve for pressure sensor with applied tiny force. (d) Relative resistance change-temperature curve for pressure sensing part(black) and temperature sensing part(red). (e) Relative resistance changes of each pressure sensing part with applied force (9.8 N) from various angle.

The stability of any designed sensors can be verified by carrying out the cyclic test for several cycles. Figure 10 shows the cycling compression test of the sensor with an applied normal force of 5 N. There is a slight drift. To the best of the authors knowledge, it is assumed that the temperature rises due to the repeated elastic deformation (Figure 10(b)). Thus, drift in the pressure sensor and temperature sensor are comparable. In addition, there is a constant change in resistance of the pressure sensor when repeated several times. Under the loading, the temperature sensor shows much smaller resistance change (Figure 10(a)).

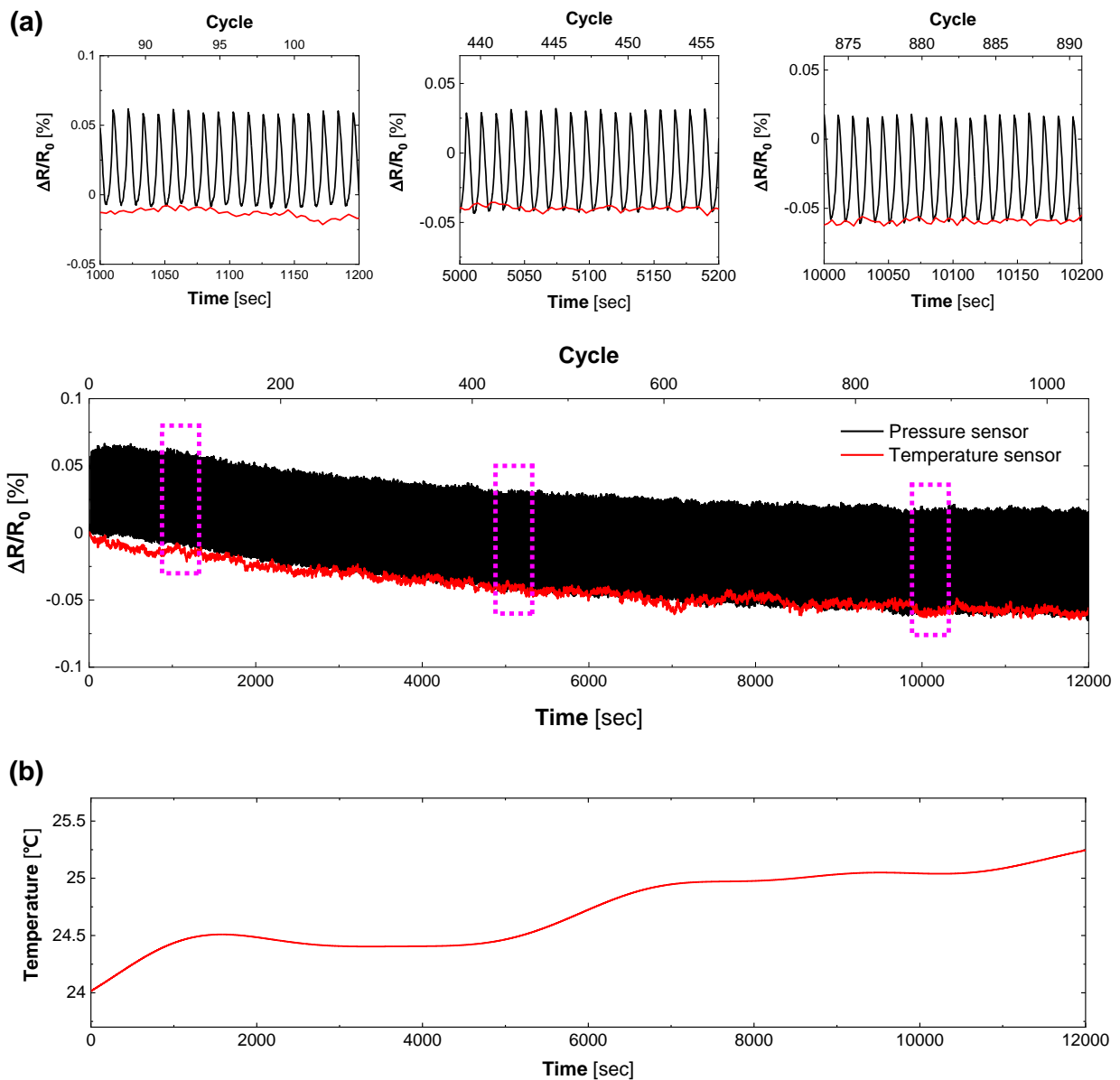
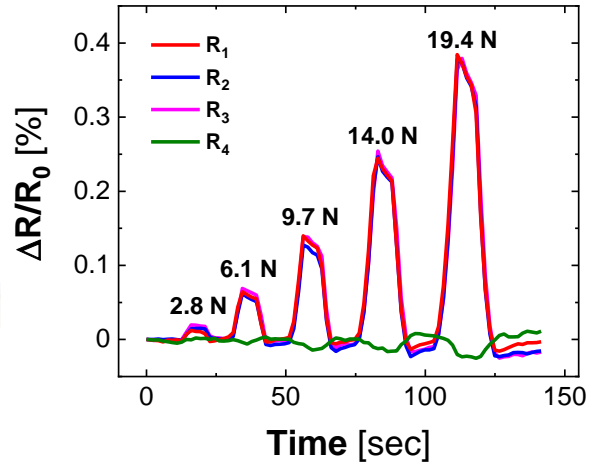
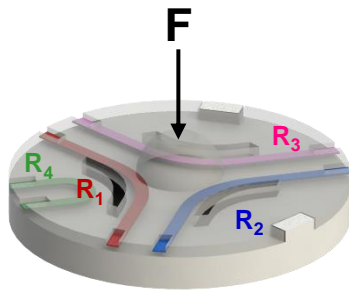


**Figure 10. Relative resistance changes of pressure sensor, temperature sensor (a) and temperature change of the entire sensor (b) applying a force of 5 N for more the 1000 cycles.**

Figure 11 shows the relative resistance change due to applied forces in  $0^\circ$  (Figure 11 (a)) and  $45^\circ$  (Figure 11 (b)) in respect to the normal direction. In the case of  $0^\circ$ , the relative resistance changes of  $R_{1-3}$  are almost the same. On the other hand, at  $45^\circ$ ,  $R_1$  has 0.319% and  $R_{2-3}$  have about 0.178% of relative resistance change 17.8 N loading. Moreover,  $R_4$ , the temperature

sensing part, has a relatively small resistance change, as it does not get affected by an external force.

**(a) Normal Force**



**(b) Tilted Force**

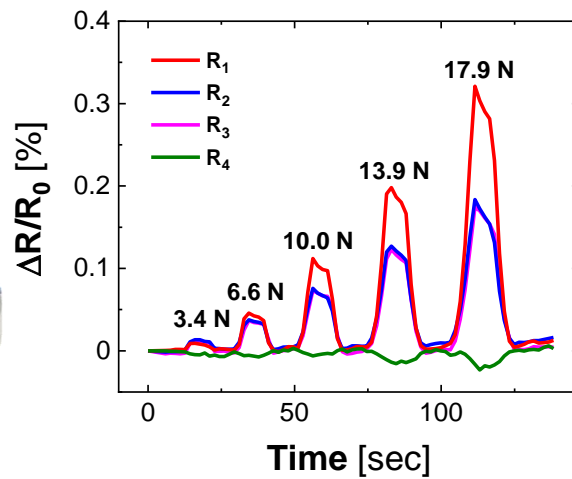
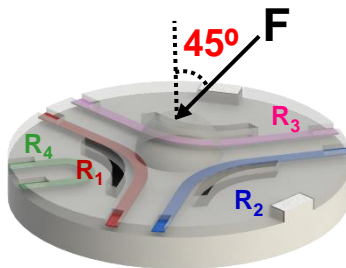
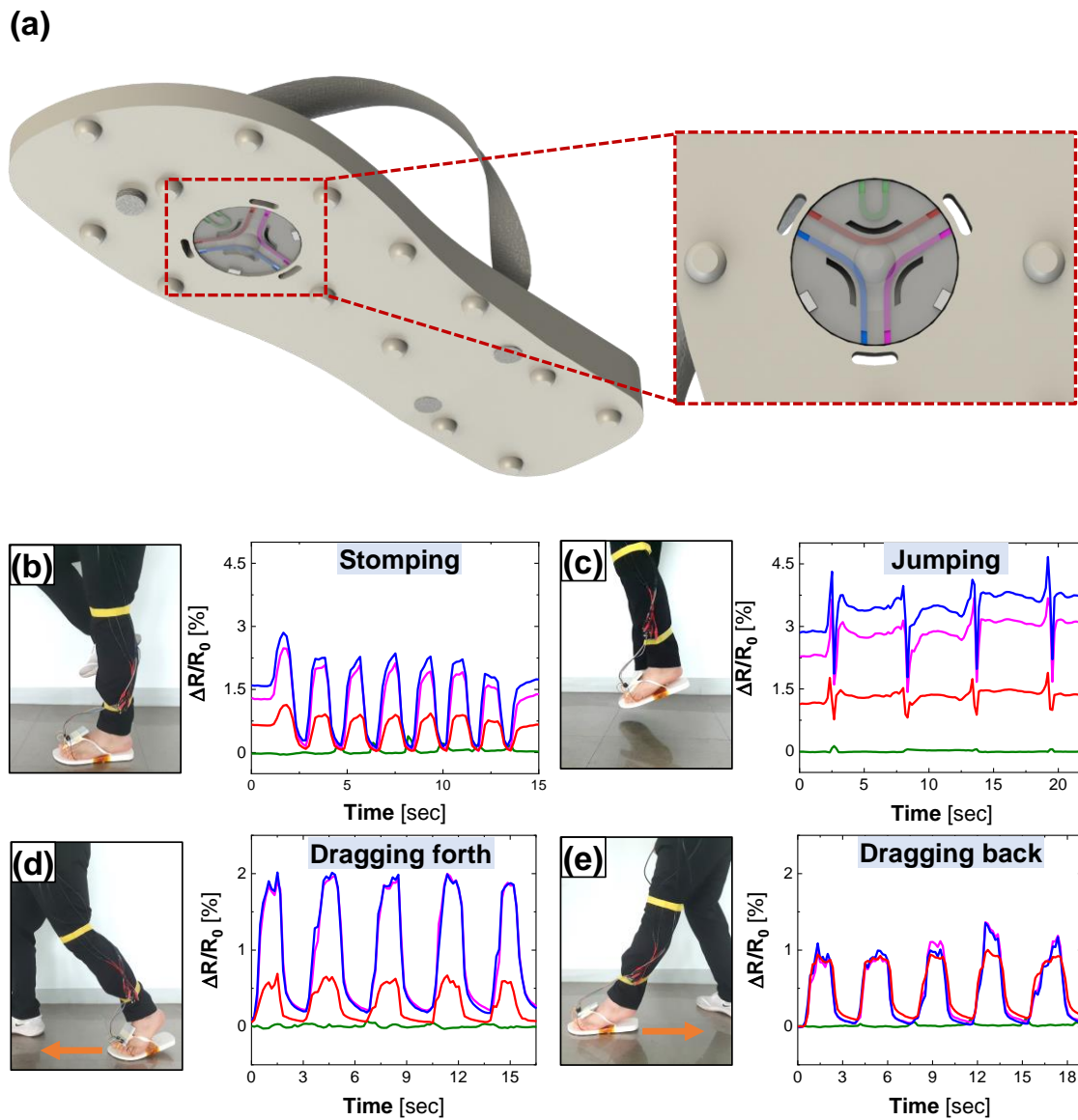


Figure 11. Multi-axis sensing performance of pressure sensor in (a) normal force, (b) tiled force.

### **3) 3D printed multi-axis pressure sensor application**

The applications of any sensor system play a vital role in realizing its usage in our daily life. The multi-axis pressure sensor can have an advantage over conventional normal pressure sensors in human gait monitoring. Figure 12 (a) shows the design of the 3D printed sensor integration with a 3D printed flip-flop. The body material of the flip-flop is TPU. The designed sensor bears a bump-like structure under the flip-flop, preventing damage to the sensor. Figure 12 (b-e) shows the sensing performance of the sensor. The resistance change in the case of daily gait activities like stomping and running is distinguished clearly. The sensing is also possible in the direction of dragging forth the flip-flop. In addition, there is a small resistance change of the temperature sensor (green line). Here, the resistance of each sensing part is slightly different because the inclination of the sole of the flip-flop and the direction of force when a person presses it is slightly different. For all gait postures, our sensor exhibits an excellent response time in the order of 100 ms.



**Figure 12. (a) Schematic of multi-axis pressure sensor integrated with flip-flop. (b-e) The sensing performance of the flip-flop.**

To extend the application of the sensor, it was integrated with the gripper as shown in Figure 13 (a). The 3D printing of the gripper is performed utilizing the TPU. Figure 13 (b) shows the sensing performance of the sensor during soft grip, hard grip, and lifting. The resistance change appears differently depending on the force to hold the object. During the lifting process, the

resistance change is higher which reflects the pressure sensing capability of the designed sensor, and the weight of the object can be further evaluated.

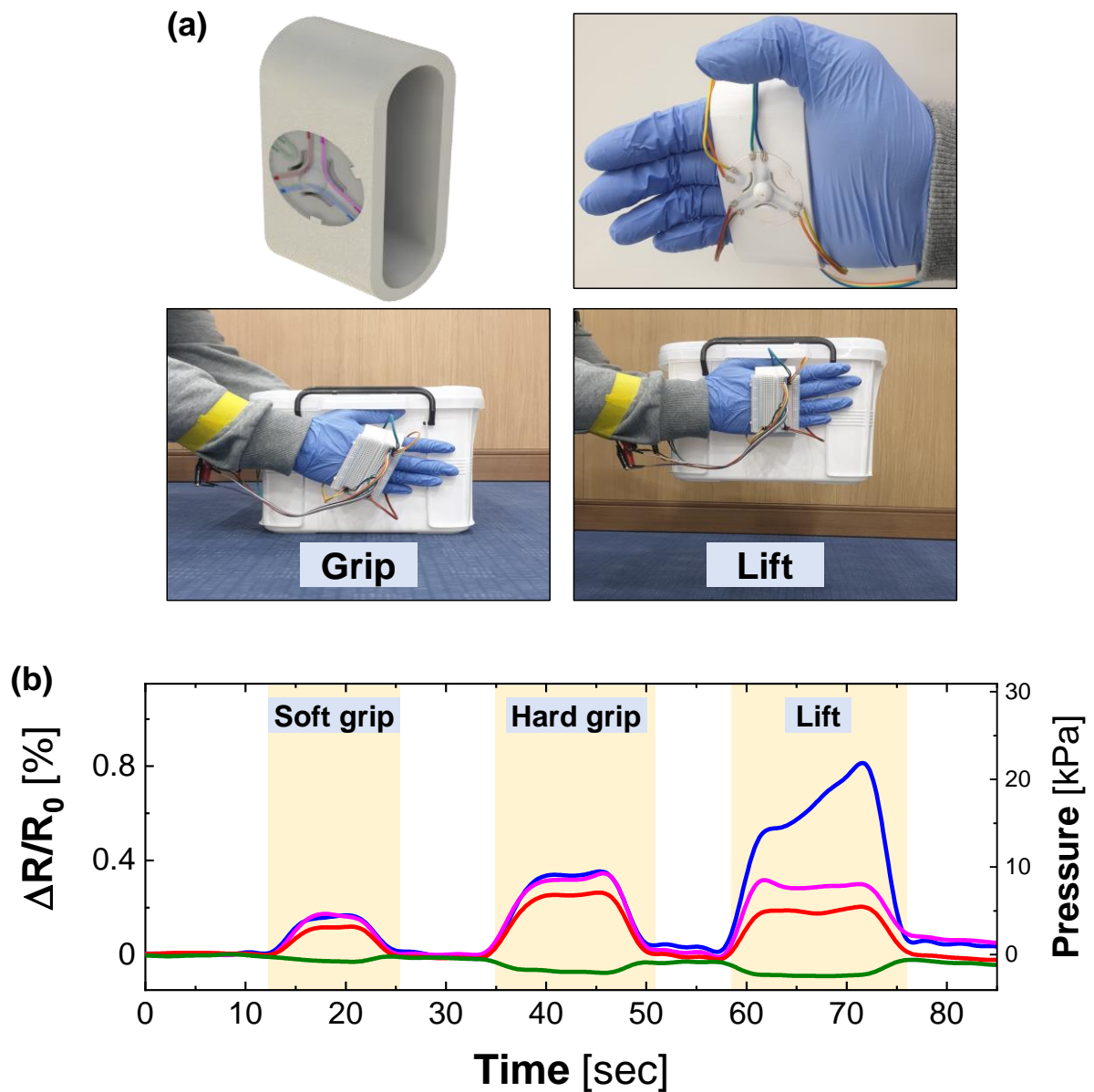


Figure 13. (a) Schematic of multi-axis pressure sensor integrated with gripper. (b) The sensing performance of the gripper.

## VI. Conclusion

This paper reports the design, fabrication, and characterization of a 3D printed multi-axis pressure sensor consisting of MWCNTs/PLA composite polymer. By controlling the MWCNTs concentration in the composite polymer, the electrical and mechanical properties of the composite can be precisely tuned. The pressure sensor along with the temperature sensor could be very beneficial to quantify mechanical forces or pressures in various applications. Furthermore, the sensor uses a bumper-spacing structure along with three pressure-sensing elements so that each sensing part can be deformed differently depending on the direction of external force. In addition, it offers the additional functionality of calibrating the resistance change with temperature using the temperature-sensing part. The bumper structure of the pressure sensors was attached to a 3D-printed flip-flop and a hand gripper to realize the readout during several human motions and grasping activities. The above results elucidate that the designed sensor could extend the functionalities towards robotic grippers and human tactile sensors. This type of cost-effective methodology of 3D printing sensors can reduce effort and aim towards large-scale production. In the future, these sensors can be combined with shoes to compare the gait of the

normal human and patients, to carry out clinical assessments. Involving machine learning technology could quantify and analyzed results obtained through these sensors for more advanced medical applications in near future. In addition, with the integration along with a robotics gripper, it can detect multi-direction shear force as well as temperature compared to conventional sensors which are capable of detecting normal direction force paves the way for development in smart robotics system in near future.

## References

- [1] M. Amit, L. Chukoskie, A. J. Skalsky, H. Garudadri, and T. N. Ng, "Flexible pressure sensors for objective assessment of motor disorders," *Advanced Functional Materials*, vol. 30, no. 20, p. 1905241, 2020.
- [2] Y. Zhou *et al.*, "Highly sensitive, self-powered and wearable electronic skin based on pressure-sensitive nanofiber woven fabric sensor," *Scientific reports*, vol. 7, no. 1, pp. 1-9, 2017.
- [3] A. Chortos and Z. Bao, "Skin-inspired electronic devices," *Materials Today*, vol. 17, no. 7, pp. 321-331, 2014.
- [4] S. Kang *et al.*, "Highly sensitive pressure sensor based on bioinspired porous structure for real-time tactile sensing," *Advanced Electronic Materials*, vol. 2, no. 12, p. 1600356, 2016.
- [5] M. Munoz-Organero, C. Littlewood, J. Parker, L. Powell, C. Grindell, and S. Mawson, "Identification of walking strategies of people with osteoarthritis of the knee using insole pressure sensors," *IEEE Sensors Journal*, vol. 17, no. 12, pp. 3909-3920, 2017.
- [6] W. Chen and X. Yan, "Progress in achieving high-performance piezoresistive and capacitive flexible pressure sensors: A review," *Journal of Materials Science & Technology*, vol. 43, pp. 175-188, 2020.
- [7] Y. Ding, T. Xu, O. Onyilagha, H. Fong, and Z. Zhu, "Recent advances in flexible and wearable pressure sensors based on piezoresistive 3D monolithic conductive sponges," *ACS applied materials & interfaces*, vol. 11, no. 7, pp. 6685-6704, 2019.
- [8] T. D. Ngo, A. Kashani, G. Imbalzano, K. T. Nguyen, and D. Hui, "Additive manufacturing (3D printing): A review of materials, methods, applications and challenges," *Composites Part B: Engineering*, vol. 143, pp. 172-196, 2018.
- [9] B. Utela, D. Storti, R. Anderson, and M. Ganter, "A review of process development steps for new material systems in three dimensional printing (3DP)," *Journal of Manufacturing Processes*, vol. 10, no. 2, pp. 96-104, 2008.
- [10] M. A. Gibson *et al.*, "3D printing metals like thermoplastics: Fused filament fabrication of metallic glasses," *Materials Today*, vol. 21, no. 7, pp. 697-702, 2018.
- [11] Y. K. Mishra *et al.*, "Direct growth of freestanding ZnO tetrapod networks for multifunctional applications in photocatalysis, UV photodetection, and gas sensing," *ACS applied materials & interfaces*, vol. 7, no. 26, pp. 14303-14316, 2015.
- [12] M. Chen *et al.*, "3D nanoprinting of perovskites," *Advanced Materials*, vol. 31, no. 44, p. 1904073, 2019.

- [13] S. Hajra, M. Sahu, V. Purohit, and R. Choudhary, "Dielectric, conductivity and ferroelectric properties of lead-free electronic ceramic: 0.6 Bi (Fe<sub>0.98</sub>Ga<sub>0.02</sub>) O<sub>3</sub>-0.4 BaTiO<sub>3</sub>," *Heliyon*, vol. 5, no. 5, p. e01654, 2019.
- [14] M. Sahu, S. Hajra, J. Bijelic, D. Oh, I. Djerdj, and H. J. Kim, "Triple perovskite-based triboelectric nanogenerator: a facile method of energy harvesting and self-powered information generator," *Materials Today Energy*, vol. 20, p. 100639, 2021.
- [15] K. Gnanasekaran *et al.*, "3D printing of CNT-and graphene-based conductive polymer nanocomposites by fused deposition modeling," *Applied materials today*, vol. 9, pp. 21-28, 2017.
- [16] G. Stano, A. Di Nisio, A. M. Lanzolla, M. Ragolia, and G. Percoco, "Fused filament fabrication of commercial conductive filaments: experimental study on the process parameters aimed at the minimization, repeatability and thermal characterization of electrical resistance," *The International Journal of Advanced Manufacturing Technology*, vol. 111, no. 9, pp. 2971-2986, 2020.
- [17] Q.-J. Sun *et al.*, "Highly sensitive and ultrastable skin sensors for biopressure and bioforce measurements based on hierarchical microstructures," *ACS applied materials & interfaces*, vol. 10, no. 4, pp. 4086-4094, 2018.
- [18] G. Y. Bae *et al.*, "Pressure/temperature sensing bimodal electronic skin with stimulus discriminability and linear sensitivity," *Advanced Materials*, vol. 30, no. 43, p. 1803388, 2018.
- [19] Y. Zang, F. Zhang, C.-a. Di, and D. Zhu, "Advances of flexible pressure sensors toward artificial intelligence and health care applications," *Materials Horizons*, vol. 2, no. 2, pp. 140-156, 2015.
- [20] K. Namsheer and C. S. Rout, "Conducting polymers: a comprehensive review on recent advances in synthesis, properties and applications," *RSC Advances*, vol. 11, no. 10, pp. 5659-5697, 2021.
- [21] S. H. Aboutalebi *et al.*, "Comparison of GO, GO/MWCNTs composite and MWCNTs as potential electrode materials for supercapacitors," *Energy & Environmental Science*, vol. 4, no. 5, pp. 1855-1865, 2011.
- [22] H. S. Patanwala, D. Hong, S. R. Vora, B. Bognet, and A. W. Ma, "The microstructure and mechanical properties of 3D printed carbon nanotube-polylactic acid composites," *Polymer Composites*, vol. 39, no. S2, pp. E1060-E1071, 2018.
- [23] X. Wei *et al.*, "3D printable graphene composite," *Scientific reports*, vol. 5, no. 1, pp. 1-7, 2015.
- [24] I. Balberg, "A comprehensive picture of the electrical phenomena in carbon black-polymer composites," *Carbon*, vol. 40, no. 2, pp. 139-143, 2002.
- [25] I. Moreno, N. Navascues, M. Arruebo, S. Irusta, and J. Santamaria, "Facile preparation of transparent and conductive polymer films based on silver nanowire/polycarbonate nanocomposites,"

- Nanotechnology*, vol. 24, no. 27, p. 275603, 2013.
- [26] H. Yuk *et al.*, "3D printing of conducting polymers," *Nature communications*, vol. 11, no. 1, pp. 1-8, 2020.
- [27] K. Chu, S.-C. Lee, S. Lee, D. Kim, C. Moon, and S.-H. Park, "Smart conducting polymer composites having zero temperature coefficient of resistance," *Nanoscale*, vol. 7, no. 2, pp. 471-478, 2015.
- [28] F. Xu *et al.*, "Recent developments for flexible pressure sensors: a review," *Micromachines*, vol. 9, no. 11, p. 580, 2018.
- [29] J. Shi *et al.*, "Multiscale hierarchical design of a flexible piezoresistive pressure sensor with high sensitivity and wide linearity range," *Small*, vol. 14, no. 27, p. 1800819, 2018.
- [30] M. Aryafar, M. Hamed, and M. Ganjeh, "A novel temperature compensated piezoresistive pressure sensor," *Measurement*, vol. 63, pp. 25-29, 2015.
- [31] G. Zhou, Y. Zhao, F. Guo, and W. Xu, "A smart high accuracy silicon piezoresistive pressure sensor temperature compensation system," *Sensors*, vol. 14, no. 7, pp. 12174-12190, 2014.
- [32] X. Wang, M. Jiang, Z. Zhou, J. Gou, and D. Hui, "3D printing of polymer matrix composites: A review and prospective," *Composites Part B: Engineering*, vol. 110, pp. 442-458, 2017.
- [33] V. G. Rocha, E. Saiz, I. S. Tirichenko, and E. García-Tuñón, "Direct ink writing advances in multi-material structures for a sustainable future," *Journal of Materials Chemistry A*, vol. 8, no. 31, pp. 15646-15657, 2020.
- [34] A. Goulas *et al.*, "Fused filament fabrication of functionally graded polymer composites with variable relative permittivity for microwave devices," *Materials & Design*, vol. 193, p. 108871, 2020.
- [35] S. Hajra, A. Tripathy, B. K. Panigrahi, and R. Choudhary, "Development and excitation performance of lead free electronic material: Eu and Fe doped Bi<sub>0.5</sub>Na<sub>0.5</sub>TiO<sub>3</sub> for filter application," *Materials Research Express*, vol. 6, no. 7, p. 076304, 2019.
- [36] A. Goyanes, A. B. Buanz, A. W. Basit, and S. Gaisford, "Fused-filament 3D printing (3DP) for fabrication of tablets," *International journal of pharmaceuticals*, vol. 476, no. 1-2, pp. 88-92, 2014.
- [37] C. Aumnate, A. Pongwisuthiruchte, P. Pattanauwat, and P. Potiyaraj, "Fabrication of ABS/graphene oxide composite filament for fused filament fabrication (FFF) 3D printing," *Advances in Materials Science and engineering*, vol. 2018, 2018.
- [38] Y. K. Mishra and R. Adelung, "ZnO tetrapod materials for functional applications," *Materials Today*, vol. 21, no. 6, pp. 631-651, 2018.
- [39] H. J. Kwon, S. Lee, and J.-H. Kim, "3D-printed pressure sensor with heterogeneous polymer material and annealing effect," in *Nano-, Bio-, Info-Tech Sensors and Wearable Systems*, 2021, vol. 11590:

International Society for Optics and Photonics, p. 115900C.

- [40] Z. Mengjuan *et al.*, "Wide linear range and highly sensitive flexible pressure sensor based on multistage sensing process for health monitoring and human-machine interfaces," 2021.
- [41] H.-G. Kim, S. Hajra, D. Oh, N. Kim, and H. J. Kim, "Additive manufacturing of high-performance carbon-composites: An integrated multi-axis pressure and temperature monitoring sensor," *Composites Part B: Engineering*, p. 109079, 2021.
- [42] F. Ning, W. Cong, J. Qiu, J. Wei, and S. Wang, "Additive manufacturing of carbon fiber reinforced thermoplastic composites using fused deposition modeling," *Composites Part B: Engineering*, vol. 80, pp. 369-378, 2015.
- [43] Y. Tao, M. Liu, W. Han, and P. Li, "Waste office paper filled polylactic acid composite filaments for 3D printing," *Composites Part B: Engineering*, p. 108998, 2021.
- [44] G. Goh, W. Toh, Y. Yap, T. Ng, and W. Yeong, "Additively manufactured continuous carbon fiber-reinforced thermoplastic for topology optimized unmanned aerial vehicle structures," *Composites Part B: Engineering*, vol. 216, p. 108840, 2021.
- [45] J. Naranjo-Lozada, H. Ahuett-Garza, P. Orta-Castañón, W. M. Verbeeten, and D. Sáiz-González, "Tensile properties and failure behavior of chopped and continuous carbon fiber composites produced by additive manufacturing," *Additive Manufacturing*, vol. 26, pp. 227-241, 2019.
- [46] Z. Wang, X. Guan, H. Huang, H. Wang, W. Lin, and Z. Peng, "Full 3D printing of stretchable piezoresistive sensor with hierarchical porosity and multimodulus architecture," *Advanced Functional Materials*, vol. 29, no. 11, p. 1807569, 2019.
- [47] K. Kim, J. Park, J.-h. Suh, M. Kim, Y. Jeong, and I. Park, "3D printing of multiaxial force sensors using carbon nanotube (CNT)/thermoplastic polyurethane (TPU) filaments," *Sensors and Actuators A: Physical*, vol. 263, pp. 493-500, 2017.
- [48] S. Z. Guo, K. Qiu, F. Meng, S. H. Park, and M. C. McAlpine, "3D printed stretchable tactile sensors," *Advanced Materials*, vol. 29, no. 27, p. 1701218, 2017.
- [49] J. Sethi *et al.*, "The effect of multi-wall carbon nanotube morphology on electrical and mechanical properties of polyurethane nanocomposites," *Composites Part A: Applied Science and Manufacturing*, vol. 102, pp. 305-313, 2017.
- [50] J.-H. Jang *et al.*, "Dispersion and property evaluation of nanocomposites by aspect ratio of MWCNT," *Composites Research*, vol. 23, no. 3, pp. 58-63, 2010.
- [51] M. Mu, E. Teblum, Ł. Figiel, G. D. Nessim, and T. McNally, "Correlation between MWCNT aspect ratio and the mechanical properties of composites of PMMA and MWCNTs," *Materials Research Express*,

- vol. 5, no. 4, p. 045305, 2018.
- [52] X. Wang, Q. Jiang, W. Xu, W. Cai, Y. Inoue, and Y. Zhu, "Effect of carbon nanotube length on thermal, electrical and mechanical properties of CNT/bismaleimide composites," *Carbon*, vol. 53, pp. 145-152, 2013.
- [53] D. Stauffer and A. Aharony, *Introduction to percolation theory*. CRC press, 2018.
- [54] J. Park, I. R. Jang, K. Lee, and H. J. Kim, "High Efficiency Crumpled Carbon Nanotube Heaters for Low Drift Hydrogen Sensing," *Sensors*, vol. 19, no. 18, p. 3878, 2019.
- [55] C. Casavola, A. Cazzato, V. Moramarco, and G. Pappaletta, "Residual stress measurement in fused deposition modelling parts," *Polymer Testing*, vol. 58, pp. 249-255, 2017.
- [56] S. Ziemian, M. Okwara, and C. W. Ziemian, "Tensile and fatigue behavior of layered acrylonitrile butadiene styrene," *Rapid Prototyping Journal*, 2015.
- [57] A. Rodríguez-Panes, J. Claver, and A. M. Camacho, "The influence of manufacturing parameters on the mechanical behaviour of PLA and ABS pieces manufactured by FDM: A comparative analysis," *Materials*, vol. 11, no. 8, p. 1333, 2018.

## 요약문

# 탄소 복합체 폴리머의 3D 프린팅 기반 온도 보상 기능이 있는 다축 압력 센서

본 논문에서 우리는 탄소 나노 튜브 복합체 폴리머의 Fused Filament Fabrication(FFF) 3D 프린팅을 사용한 온도 보상이 가능한 다축 압력센서의 설계, 제작, 및 특성분석을 보고한다. 3D 프린팅 기술은 복잡한 삼차원 구조체를 보다 쉽고 간편하게 제작할 수 있다. 또한 전도성 폴리머의 3D 프린팅은 기계적 유연함과 함께 전기적 특성을 동시에 제공하기 때문에 유연한 전자 기기 제작에 매우 적합한 기술로 많은 연구가 이루어지고 있다. 우리는 본 연구에서 FFF 3D 프린팅을 이용하여 온도 보상이 가능한 다축 압력센서를 제작하고 이를 모션 센싱 어플리케이션에 결합하였다. 압력 감지 메커니즘은 압저항 방식을 이용하고 온도 감지는 복합체의 온도에 따른 저항 변화로 감지한다. 압력 감지부는 범퍼 구조로 되어 있어 외력이 가해질 때 기계적인 변형을 받아 저항이 변화하고, 온도 센서는 외력에 의한 기계적 변형이 없이 오로지 온도에 의해서만 저항이 변화한다. 여기서 전도성 폴리머는 polylactic acid (PLA), multi-walled carbon nanotubes (MWCNTs), 그리고 dichloromethane(DCM) 용매를 이용한 용액 캐스팅 방법을 사용하고, 최종적으로 3D 프린팅을 위한 필라멘트로 제작한다. 본 연구에서 제안하

는 센서는 외력의 크기와 방향을 측정하여 정량화 할 수 있을 뿐 아니라, 온도에 따른 저항보상도 가능하게 한다. 이러한 온도 보상이 가능한 다축 압력 센서는 모션 모니터링 시스템 등 다양한 어플리케이션에 적용될 수 있다.

핵심어: 3D 프린팅, 탄소 복합체, 압력 센서, 다축 감지, 온도 보상